Natural Convection Flow past a Vertical Truncated Cone in Porous Media Filled with Nanofluids

Kuo-Ann Yih, Heng-Pin Hsu, Ken-Ming Tu, Uon-Jien Payne, Ming-Shen Sheu

Department of Aircraft Engineering, Air Force Institute of Technology

Abstract

The natural convection flow past a vertical truncated cone in porous media filled with nanofluids is numerically analyzed in this paper. The transformed conservation equations governing the nonsimilar boundary layers are solved by the Keller box method (KBM). Numerical results for the dimensionless temperature profiles and the reduced Nusselt number are graphically and tabularly presented for the dimensionless distance ξ and the nanoparticles volume fraction φ (three nanoparticles are considered). Increasing the value of dimensionless distance ξ increases the reduced Nusselt number. Moreover, the reduced Nusselt number approaches to the limit of the inclined plate (full cone) as dimensionless distance ξ is very small (large). However, enhancing the nanoparticles volume fraction φ decreases the reduced Nusselt number. For the case of Cu-nanoparticles (Al₂O₃-nanoparticles), the reduced Nusselt number is higher (lower).

Keywords: natural convection, vertical truncated cone, porous media, nanofluids

飽和多孔性介質內充滿奈米流體之垂直截尾圓錐體自然對流

易國安,許恒斌,杜耿銘,潘永堅,徐明生

空軍航空技術學院 飛機工程系

摘 要

在本文中吾人使用數值解法以探討在飽和多孔性介質內充滿奈米流體之垂直截尾圓錐體自然對流。偏微分方程式經轉換成非相似邊界層方程式後,再以凱勒盒子法解之。數值計算結果主要以圖表來顯示:無因次距離、奈米粒子體積分率(考慮三種奈米粒子)對無因次溫度分佈與縮減的紐賽數之影響。增加無因次距離,則增強縮減的紐賽數。此外,當無因次距離非常小(大)時,縮減的紐賽數趨近於傾斜平板(完全錐體)之極限情況。然而,增大奈米粒子體積分率,降低縮減的紐賽數。對於銅-奈米粒子(三氧化二鋁),縮減的紐賽數為較高(較低)。

關鍵詞:自然對流,垂直截尾圓錐體,飽和多孔性介質,奈米流體

1. Introduction

The problem of convective heat transfer in a saturated porous medium has many important applications in geothermal system and geophysical engineering such as enhanced recovery of petroleum resources, nuclear reactor cooling system and underground disposal of nuclear wastes, as reported by Nield and Bejan [1].

Cheng et al. [2] studied the natural convection of a Darcian fluid about a cone. Coupled heat and mass transfer by free convection over a truncated cone in porous media: variable wall temperature/variable wall concentration (VWT/VWC) or variable heat flux/variable mass flux (VHF/VMF) was analyzed by Yih [3]. Chamkha et al. [4] examined free convection flow over a truncated cone embedded in a porous medium saturated with pure or saline water at low temperatures. Cheng [5] investigated natural convection heat and mass transfer from a vertical truncated cone in a porous medium saturated with a non-Newtonian fluid with variable wall temperature and concentration. Double-diffusive convection with variable viscosity from a vertical truncated cone in porous media in the presence of magnetic field and radiation effects was reported by Mahdy et al. [6]. Yih and Huang [7] studied effect of internal heat generation on free convection flow of non-Newtonian fluids over a vertical truncated cone in porous media for the case VWT/VWC. Amanulla et al. [8] investigated thermal and momentum slip effects on hydromagnetic convection flow of a Williamson fluid past a vertical truncated cone. Tu et al. [9] analyzed Taguchi method numerical simulation for variable and

viscosity and non-linear Boussinesq effects on natural convection over a vertical truncated cone in porous media.

Nanotechnology application is in sciences, physical biological sciences. electronic cooling, and advanced nuclear systems. An innovative technique improving heat transfer by using ultra fine solid particles in the fluids has been used extensively during the last several years. Choi [10] is the first who used the term "nanofluids" to refer to the fluid containing a suspension of submicronic solid particles (nanoparticles). Buongiorno [11] made a comprehensive survey of convection in nanofluids and wrote down the conservation equations for nanofluids involving both the Brownian motion and thermophoresis effects. Recently, review of convection heat transfer and fluid flow in porous media with nanofluid was made by Kasaeian et al. [12]. Cheng [13] studied free convection of non-Newtonian nanofluids about a vertical truncated cone in a porous medium. Free convection of a nanofluid about a vertical truncated cone was analyzed by Cheng [14] for zero nanoparticle flux. In both of these papers [13-14] the authors have used the nanofluid model proposed by Buongiorno [11]. Although this author discovered that seven slip mechanisms take place convective transport in nanofluids, it is only the **Brownian** diffusion and the thermophoresis that are the most important when the turbulent flow effects are absent.

Oztop and Abu-Nada [15] used another model of nanofluid to study natural convection in partially heated rectangular enclosures filled with nanofluids based on the real thermophysical properties of fluid and nanoparticles. Ahmad and Pop [16] examined mixed convection boundary layer flow from a vertical flat plate embedded in a porous medium filled with nanofluids. Boundary-layer flow over a porous medium of a nanofluid past from a vertical cone was investigated by Mohammad and Jamaladin [17]. EL-Kabeir et al. [18] discussed effect of thermal radiation on non-Darcy natural convection from a vertical cylinder embedded in a nanofluid porous media. Waini et al. [19] analyzed mixed convection of a hybrid nanofluid flow along a vertical surface embedded in a porous medium.

The objective of the present work, therefore, is to extend the work of Cheng et al. [2] and another model of nanofluid [15] to consider the natural convection flow past an isothermal vertical truncated cone embedded in a porous medium filled with nanofluids.

2. Analysis

Let us consider the problem of the two-dimensional, steady, laminar free convection boundary layer flow past a vertical truncated cone (with half angle γ) embedded in a saturated porous medium filled with nanofluids. Figure 1 shows the flow model and physical coordinate system. The origin of the coordinate system is placed at the vertex of the vertical full cone, where x and y are coordinates measured along and normal to the vertical truncated cone surface, respectively. The radius of the vertical truncated cone is r. The uniform wall temperature of the vertical truncated cone T_w is higher than the ambient temperature T_∞ . The physical properties of the nanofluid are considered to be constant except for the density variation in the body force term.

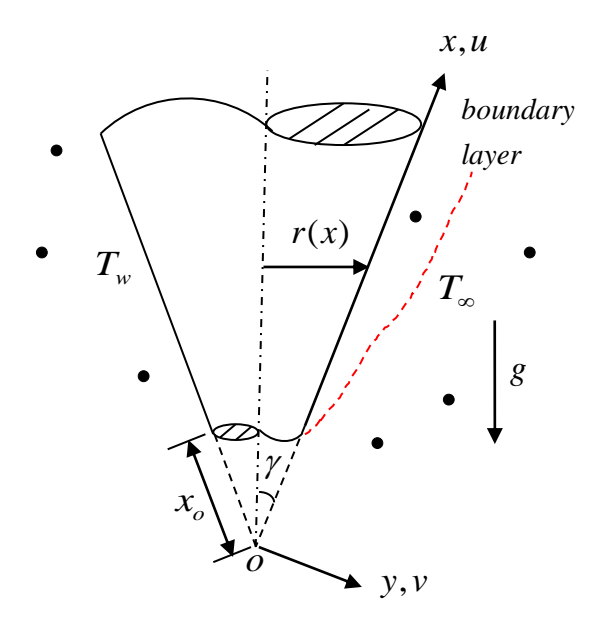


Fig. 1. The flow model and physical coordinate system

Introducing the spherical nanofluid model proposed by Oztop and Abu-Nada [15], the boundary layer approximation and Boussinesq approximation, the governing equations and the boundary conditions based on the Darcy law can be written as follows:

$$\frac{\partial(ru)}{\partial x} + \frac{\partial(rv)}{\partial y} = 0,\tag{1}$$

$$\frac{\partial u}{\partial y} = \frac{(\rho \beta)_{nf} g \cos \gamma K}{\mu_{nf}} \frac{\partial T}{\partial y}, \qquad (2)$$

$$u\frac{\partial T}{\partial x} + v\frac{\partial T}{\partial y} = \alpha_{nf} \frac{\partial^2 T}{\partial y^2}.$$
 (3)

$$y = 0$$
: $v = 0$, $T = T_w$, (4)

$$y \to \infty$$
: $u = 0$, $T = T_{\infty}$. (5)

where u and v are the Darcian velocities in the x- and y- directions, respectively. g is the gravitational acceleration. K is the permeability of the porous medium. Tis the temperature.

The thermal expansion coefficient of the nanofluid $(\rho\beta)_{nf}$ is given by:

$$(\rho\beta)_{nf} = (1 - \varphi)(\rho\beta)_f + \varphi(\rho\beta)_s \tag{6}$$

The dynamic viscosity of the nanofluid μ_{nf} is determined by:

$$\frac{\mu_{nf}}{\mu_f} = \frac{1}{(1 - \varphi)^{2.5}} \tag{7}$$

The thermal diffusivity of the nanofluid α_{nf} is defined as:

$$\alpha_{nf} = \frac{k_{nf}}{\left(\rho C_p\right)_{nf}} \tag{8}$$

with

$$\frac{k_{nf}}{k_f} = \frac{\left(k_s + 2k_f\right) - 2\varphi\left(k_f - k_s\right)}{\left(k_s + 2k_f\right) + \varphi\left(k_f - k_s\right)} \tag{9}$$

$$\left(\rho C_{p}\right)_{nf} = \left(1 - \varphi\right)\left(\rho C_{p}\right)_{f} + \varphi\left(\rho C_{p}\right)_{s} \qquad (10)$$

Here, φ is the solid volume fraction parameter; ρ_f and ρ_s are the densities of the basic fluid and the nanoparticle, respectively; β_f and β_s are the thermal expansion coefficients of the base fluid and the nanoparticle, respectively; μ_f is the

dynamic viscosity of the basic fluid; k_{nf} and $(\rho C_P)_{nf}$ are the thermal conductivity and the heat capacitance of nanofluid, respectively; k_f and k_s are the thermal conductivity of the base fluid and the nanoparticles, respectively; $(\rho C_P)_f$ and $(\rho C_P)_s$ are the heat capacitance of the base fluid and the nanoparticles, respectively. The thermophysical properties of the nanofluid are given in Table 1.

Table 1. Thermophysical properties of fluid and nanoparticles (Oztop and Abu-Nada

[15]). Physical Fluid Cu Al_2O_3 TiO₂ phase properties (water) 4179 385 765 686.2 C_P (J/kg K) ρ (kg/m³) 997.1 8933 3970 4250 400 8.9538 k (W/m K) 0.613 40 21 1.67 0.85 0.9 $\beta \times 10^{-5} \, (1/K)$

The boundary layer is assumed to be sufficiently thin in comparison with the local radius of the vertical truncated cone. The local radius to a point in the boundary layer, therefore, can be replaced by the radius of the vertical truncated cone, i.e., $r = x \sin \gamma$. Eqs. (1)—(5) are valid in $x_o \le x < \infty$ where x_o is the distance of the leading edge of vertical truncated cone measured from the origin.

Defining a stream function ψ such that

$$ru = \frac{\partial \psi}{\partial v}, \qquad rv = -\frac{\partial \psi}{\partial x}.$$
 (11)

Eq. (1), i.e., continuity equation is then automatically satisfied.

Using the following dimensionless variables

$$\xi = \frac{x^*}{x_o} = \frac{x - x_o}{x_o}$$
 (12)

$$\eta = \frac{y}{x^*} Ra_{x^*}^{1/2}$$
 (13)

$$f(\xi,\eta) = \frac{\psi}{\alpha_f r Ra_{\bullet}^{\frac{1}{2}}} \tag{14}$$

$$\theta(\xi,\eta) = \frac{T - T_{\infty}}{T_{w} - T_{\infty}} \tag{15}$$

$$Ra_{x^*} = \frac{g\cos\gamma\beta_f K(T_w - T_\infty)x^*}{v_f \alpha_f}$$
 (16)

and substituting Eqs. (6) - (16) into Eqs. (1)-(5), we can obtain the dimensionless governing equations and the boundary conditions

$$\frac{1}{(1-\varphi)^{2.5}} f' = \left[1 - \varphi + \varphi \frac{(\rho\beta)_s}{(\rho\beta)_f} \right] \theta \qquad (17)$$

$$\frac{k_{nf}/k_{f}}{\left[1-\varphi+\varphi(\rho C_{P})_{s}/(\rho C_{P})_{f}\right]}\theta'' + \left(\frac{\xi}{1+\xi} + \frac{1}{2}\right)f\theta' = \xi\left(f'\frac{\partial\theta}{\partial\xi} - \theta'\frac{\partial f'}{\partial\xi}\right).$$
(18)

$$\eta = 0$$
: $f = 0$, $\theta = 1$, (19)

$$\eta_{\infty} \to \infty: \qquad \theta = 0.$$
(20)

In the above equations, the primes denote the differentiation with respect to η . Eq. (17) is obtained by integrating Eq. (2)

once with the help of Eq. (5). α_f is the

thermal diffusivity of the base fluid. Ra_{x^*} is

the modified local Rayleigh number based upon x^* (the distance measured from the leading edge of the vertical truncated cone).

In terms of the new variables, the Darcian velocities in x- and y- directions are given by

$$u = \frac{\alpha_f R a_{x^*}}{x^*} f', \qquad (21)$$

$$v = -\frac{\alpha_f R a_{x}^{\frac{1}{2}}}{x^*} \left[\left(\frac{\xi}{1+\xi} + \frac{1}{2} \right) f + \xi \frac{\partial f}{\partial \xi} - \frac{1}{2} \eta f' \right]. \tag{22}$$

For the engineering practical applications, it is the local Nusselt number that is of interest and is given by

$$Nu_{x^*} = \frac{h_f x^*}{k_f} = \frac{q_w x^*}{k_f (T_w - T_\infty)}.$$
 (23)

where h_f denotes the local heat transfer coefficient. The rate of heat transfer q_w at the surface of the vertical truncated cone is

$$q_{w} = -k_{nf} \frac{\partial T}{\partial y} \bigg|_{y=0} \tag{24}$$

Substituting Eqs. (12)—(16), (24) into Eq. (23), we get the reduced Nusselt number

 $Nu_{x^*}/Ra_{y^*}^{1/2}$ (see Nield and Kuznetsov [20])

$$\frac{Nu_{x^*}}{Ra_{x^*}^{\frac{1}{2}}} = \frac{k_{nf}}{k_f} \left[-\theta'(\xi, 0) \right]. \tag{25}$$

It is apparent that for the case of $\varphi=0$ (regular fluid-porous medium), Eqs. (17)—(20) are reduced to those of Cheng et al. [2]. For the case of $\xi=\gamma=0$ ($\xi\to\infty$), Eqs. (17)—(20) are reduced to the vertical plate (vertical full cone) and the similarity solutions are obtained (as $\xi\to\infty$, $\partial f/\partial \xi=\partial\theta/\partial \xi=0$)

3. Numerical method

The present analysis integrates the system of equations (17)—(20) by the Keller box method (KBM) of Cebeci and Bradshaw [21]. To begin with, the partial differential equations are first converted into a system of three first-order equations. Then these first-order equations are expressed in finite difference forms and solved along with their boundary conditions by an iterative scheme.

The computations were carried out on a personal computer. The variable grid parameter is 1.01, $\Delta\eta_1 = 0.01$, $\eta_\infty = 20$, and $\Delta\xi = 0.001$ ($0 \le \xi \le 0.01$), 0.01 ($0.01 \le \xi \le 0.1$), 0.1 ($0.1 \le \xi \le 1$), 1 ($1 \le \xi \le 10$), 10 (10 $1 \le \xi \le 10$), 100 (100 $1 \le \xi \le 100$). The iterative procedure is stopped to give the temperature distribution when the error in computing the θ_w' in the next procedure becomes less than 10^{-5} .

4. Results and discussion

In order to check the accuracy of our computer simulation model, we have compared our results with those of Cheng et al. [2] and Tu et al. [9]. Table 2 lists the comparison result of the values of $-\theta'(\xi,0)$ in the absence of the nanoparticles ($\varphi=0$). It is found that the values of $-\theta'(\xi,0)$ of Cheng et al. [2] are overestimated by the local nonsimilarity solution (LNS). The difference is due to the derivatives of certain terms are discarded in the local nonsimilarity solution.

Table 2. Comparison of $-\theta'(\xi,0)$ at $\varphi=0$

			•
ξ	Cheng et al.	Tu et al.	Present
	[2]	[9]	results
0.0	0.4437	0.4437	0.4437
0.001		0.4440	0.4440
0.01	_	0.4458	0.4459
0.1	_	0.4647	0.4647
0.5	0.5412		0.5286
1	0.5991	0.5807	0.5808
2	0.6572	0.6372	0.6373
4		0.6895	0.6895
6	0.7219	0.7123	0.7123
8		0.7250	0.7250
10	0.7391	0.7330	0.7330
20	0.7532		0.7500
40	0.7607		0.7591
100	_	0.7648	0.7648
1000	_	0.7682	0.7682
10^{4}	0.7685	0.7685	0.7685

Numerical results are presented in the graphical and tabular forms for the dimensionless distance ξ ranging from 0 to 10000, and nanoparticles volume fraction φ varying from 0 to 0.3. In this study, three nanoparticles are Copper (Cu), Alumina

(Al₂O₃), and Titanium oxide (TiO₂), when the base fluid is water.

Figure 2 illustrates the dimensionless temperature profiles for three values of φ with Cu-Water, $\xi = 1$. As the nanoparticles volume fraction φ increases, both the dimensionless temperature profiles $\theta(\xi, \eta)$ and the thermal boundary layer thickness δ_T increase, yet the dimensionless wall temperature gradient $[-\theta'(\xi,0)]$ decreases.

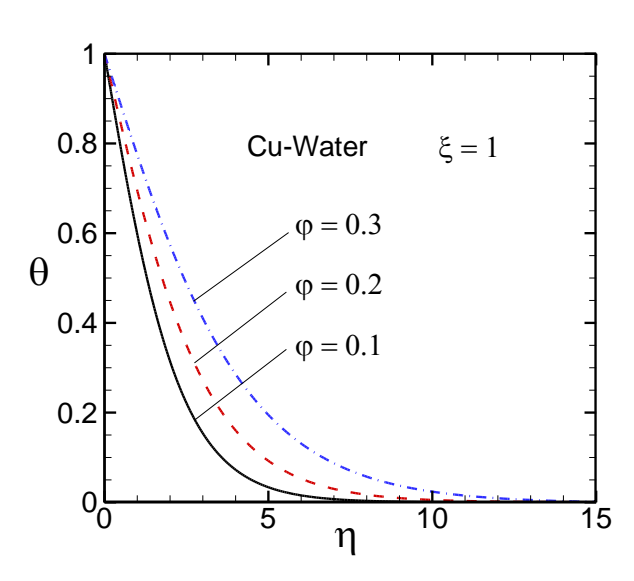


Fig. 2. Dimensionless temperature profiles for three values of φ with Cu-Water, $\xi = 1$

Table 3 displays the values of reduced

Nusselt number $Nu_{x^*}/Ra_{x^*}^{\frac{1}{2}}$ for various values of ξ and φ in the case of Cu-Water. On the one hand, for the fixed φ , the reduced Nusselt number $Nu_{x^*}/Ra_{x^*}^{\frac{1}{2}}$ enhances with increasing the dimensionless distance ξ . This is because an increase in the value of the dimensionless distance ξ implies the increase of the buoyancy force

which tends to accelerate the flow. It is also

revealed that the reduced Nusselt number approaches to constant value when ξ is very small and large.

On the other hand, at a given ξ , an increase in the value of the nanoparticles volume fraction φ leads to decreasing the reduced Nusselt number $Nu_{x^*}/Ra_{x^*}^{\frac{1}{2}}$. This is on account of the fact increasing the nanoparticles volume fraction φ reduces the value of k_{nf}/k_f , as seen from Eq. (9), and decreases the dimensionless temperature gradient $[-\theta'(\xi,0)]$, as shown in Fig. 2. Therefore, the reduced Nusselt $Nu_{*} / Ra_{*}^{\frac{1}{2}}$ number decreases with increasing the nanoparticles volume fraction φ , with the help of (25).

Table 3. Values of $Nu_{x^*} / Ra_{x^*}^{\frac{1}{2}}$ for various values of ξ and φ in the case of Cu-Water

ζ	$Nu_{x^*}/Ra_{x^*}^{y_2}$			
9	$\varphi = 0.1$	$\varphi = 0.2$	$\varphi = 0.3$	
0	0.3293	0.2424	0.1756	
0.001	0.3295	0.2425	0.1757	
0.01	0.3309	0.2436	0.1764	
0.1	0.3448	0.2538	0.1838	
1	0.4310	0.3172	0.2295	
5	0.5215	0.3838	0.2775	
10	0.5440	0.4003	0.2894	
100	0.5675	0.4177	0.3019	
1000	0.5701	0.4195	0.3033	
10^{4}	0.5703	0.4197	0.3034	

Dimensionless temperature profiles for three nanoparticles with $\xi = 10000$, $\varphi = 0.3$ are illustrated in Fig. 3. This figure depicts that by using three types of nanofluid as the

value of the dimensionless temperature profiles is lower (larger) for the case of the Cu-nanoparticles (Al₂O₃-nanoparticles).

The values of the reduced Nusselt number $Nu_{x^*}/Ra_{x^*}^{\frac{1}{2}}$ for various values of φ and three nanoparticles with (a) $\xi = 0$ (b) $\xi = 1$ (c) $\xi = 10^4$ are displayed in Table 4. For the fixed ξ and φ , it is observed that the reduced Nusselt number is higher (lower) for the Cu-nanoparticles case of (Al₂O₃-nanoparticles). This is because for Cu-nanoparticles case, the dimensionless temperature profiles is lower and the dimensionless wall temperature gradient is greater, as shown in Fig. 4. The greater the dimensionless wall temperature gradient, the larger the reduced Nusselt number.

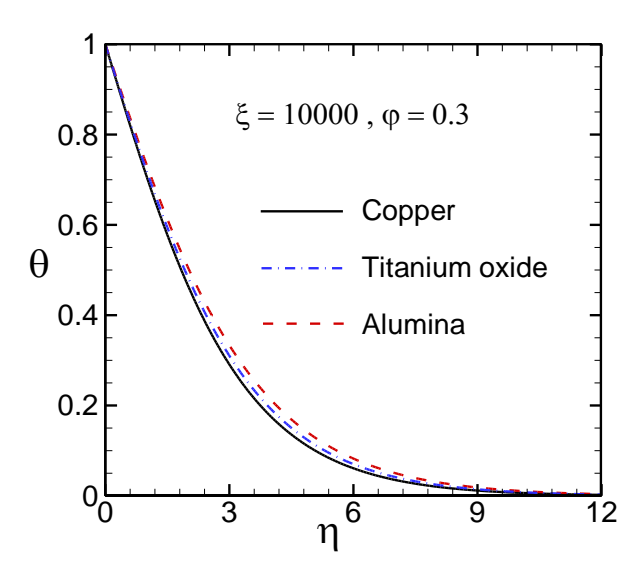


Fig. 3. Dimensionless temperature profiles for three nanoparticles with $\xi = 10000$, $\varphi = 0.3$

Table 4. Values of $Nu_{x^*}/Ra_{x^*}^{\frac{1}{2}}$ for various

values of φ and three nanoparticles with

(a)
$$\xi = 0$$
 (b) $\xi = 1$ (c) $\xi = 10^4$

(a) $\xi = 0$	$Nu_{x^*}/Ra_{x^*}^{\frac{1}{2}}$			
φ	Cu	TiO ₂	Al ₂ O ₃	
0.05	0.3824	0.3809	0.3772	
0.1	0.3293	0.3261	0.3200	
0.15	0.2830	0.2783	0.2706	
0.2	0.2424	0.2366	0.2279	
0.25	0.2068	0.2003	0.1910	
0.3	0.1756	0.1691	0.1593	
(b) $\xi = 1$	$Nu_{x^*} / Ra_{x^*}^{\frac{1}{2}}$			
φ	Cu	TiO ₂	Al_2O_3	
0.05	0.5005	0.4983	0.4937	
0.1	0.4310	0.4266	0.4188	
0.15	0.3703	0.3640	0.3542	
0.2	0.3172	0.3093	0.2983	
0.25	0.2705	0.2616	0.2498	
0.3	0.2295	0.2202	0.2080	
(c) $\xi = 10^4$	$Nu_{x^*} / Ra_{x^*}^{\frac{1}{2}}$			
φ	Cu	TiO ₂	Al_2O_3	
0.05	0.6623	0.6596	0.6533	
0.1	0.5703	0.5647	0.5542	
0.15	0.4901	0.4818	0.4687	
0.2	0.4197	0.4092	0.3947	
0.25	0.3579	0.3456	0.3304	
0.3	0.3034	0.2901	0.2748	

5. Conclusions

The effect of the nanoparticles volume fraction on free convection over a vertical truncated cone embedded in a saturated porous medium is numerically analyzed. The surface is maintained at uniform wall temperature. The nonlinear boundary-layer equations were transformed and the resulting non-similarity equations were solved by an implicit finite difference scheme (Keller box method: KBM). The decay of the dimensionless temperature profiles has been observed in all cases. When the dimensionless distance ξ increases, the reduced Nusselt number also increases. Furthermore, the reduced Nusselt number of the vertical truncated cone approaches that of inclined plate (vertical full cone) for the case of $\xi = 0$ ($\xi \to \infty$). The reduced Nusselt number reduces with increasing nanoparticles volume fraction φ . It is also found that the reduced Nusselt number is (lower) higher for the case of Cu-nanoparticles (Al₂O₃-nanoparticles).

References

- [1] Nield D. A., and Bejan, A., Convection in porous media, 5th edn. Springer, New York (2017).
- [2] Cheng, P., Le, T. T., and Pop, I., "Natural convection of a Darcian fluid about a cone," International Communications in Heat and Mass Transfer, Vol. 12, pp. 705–717 (1985).
- [3] Yih, K. A., "Coupled heat and mass transfer by free convection over a truncated cone in porous media: VWT/VWC or VHF/VMF," Acta Mechanica, Vol. 137, pp. 83–97 (1999).
- [4] Chamkha, A. J., Bercea, C., and Pop, I., "Free convection flow over a truncated cone embedded in a porous medium saturated with pure or saline water at low temperatures," Mechanics Research Communications, Vol. 33, pp. 433–440 (2006).
- [5] Cheng, C. Y., "Natural convection heat and mass transfer from a vertical truncated cone in a porous medium saturated with a non-Newtonian fluid

- with variable wall temperature and concentration," International Communications in Heat and Mass Transfer, Vol. 36, pp. 585–589 (2009).
- [6] Mahdy, A., Chamkha, A. J., and Baba, Y., "Double-diffusive convection with variable viscosity from a vertical truncated cone in porous media in the presence of magnetic field and radiation effects," Computers and Mathematics with Applications, Vol. 59, pp. 3867–3878 (2010).
- [7] Yih, K. A., and Huang, C. J., "Effect of internal heat generation on free convection flow of non-Newtonian fluids over a vertical truncated cone in porous media: VWT/VWC," Journal of Air Force Institute of Technology, Vol. 14, pp. 1–18 (2015).
- [8] Amanulla, C. H., Nagendra, N., and Suryanarayana Reddy, M., "Thermal and momentum slip effects on hydromagnetic convection flow of a Williamson fluid past a vertical truncated cone," Frontiers in Heat and Mass Transfer, Vol. 9, pp. 1–9 (2017).
- [9] Tu, K. M., Yih, K. A., Chou, F. I., and Chou, J. H., "Taguchi method and numerical simulation for variable viscosity and non-linear Boussinesq effects on natural convection over a vertical truncated cone in porous media," Energies MDPI, Vol. 13, pp. 1–19 (2020).
- [10] Choi, S. U. S., "Enhancing thermal conductivity of fluids with nanoparticle," in: D. A. Siginer, H. P. Wang (Eds.), Developments and

- Applications of Non-Newtonian Flows, ASME FED, Vol. 66, pp. 99–105 (1995).
- [11] Buongiorno, J., "Convective transport in nanofluids," ASME Journal of Heat Transfer, Vol. 128, pp. 240–250 (2006).
- [12] Kasaeian, A., Daneshazarian, R., Mahian, O., Kolsi, L., Chamkha, A. J., Wongwises, S., and Pop, I., "Nanofluid flow and heat transfer in porous media: a review of the latest developments," International Journal of Heat and Mass Transfer, Vol. 107, pp. 778–791 (2017).
- [13] Cheng, C. Y., "Free convection of non-Newtonian nanofluids about a vertical truncated cone in a porous medium," International Communications in Heat and Mass Transfer, Vol. 39, pp. 1348–1353 (2012).
- [14] Cheng, C. Y., "Free convection of a nanofluid about a vertical truncated cone," Journal of the Chinese Society of Mechanical Engineers, Vol. 37, pp. 213–219 (2016).
- [15] Oztop, H. F., and Abu-Nada, E., "Numerical study of natural convection in partially heated rectangular enclosures filled with nanofluids," International Journal of Heat and Fluid Flow, Vol. 29, pp. 1326–1336 (2008).
- [16] Ahmad, S., and Pop, I., "Mixed convection boundary layer flow from a vertical flat plate embedded in a porous medium filled with nanofluids," International Communications in Heat and Mass Transfer, Vol. 37, pp. 987–991 (2010).
- [17] Mohammad, M. K., and Jamaladin, H.,

- "Boundary-layer flow over a porous medium of a nanofluid past from a vertical cone," International Journal of Innovative Research in Science & Engineering, ISSN (Online) 2347-3207, Vol. 2, pp. 383–390 (2014).
- [18] EL-Kabeir, S. M. M., Chamkha, A. J., and Rashad A. M., "Effect of thermal radiation on non-Darcy natural convection from a vertical cylinder embedded in a nanofluid porous media," Journal of Porous Media, Vol. 17, pp. 269–278 (2014).
- [19] Waini, I., Ishak, A., Groşan, T., and Pop, I., "Mixed convection of a hybrid nanofluid flow along a vertical surface embedded in a porous medium," International Communications in Heat and Mass Transfer, Vol. 114, 104565, pp. 1–5 (2020).
- [20] Nield, D. A., and Kuznetsov, A. V., "The Cheng-Minkowycz problem for natural convective boundary-layer flow in a porous medium saturated by a nanofluid," International Journal of Heat and Mass Transfer, Vol. 52, pp. 5792–5795 (2009).
- [21] Cebeci, T., and Bradshaw, P., Physical and Computational Aspects of Convective Heat Transfer, New York, Springer-Verlag (1984).